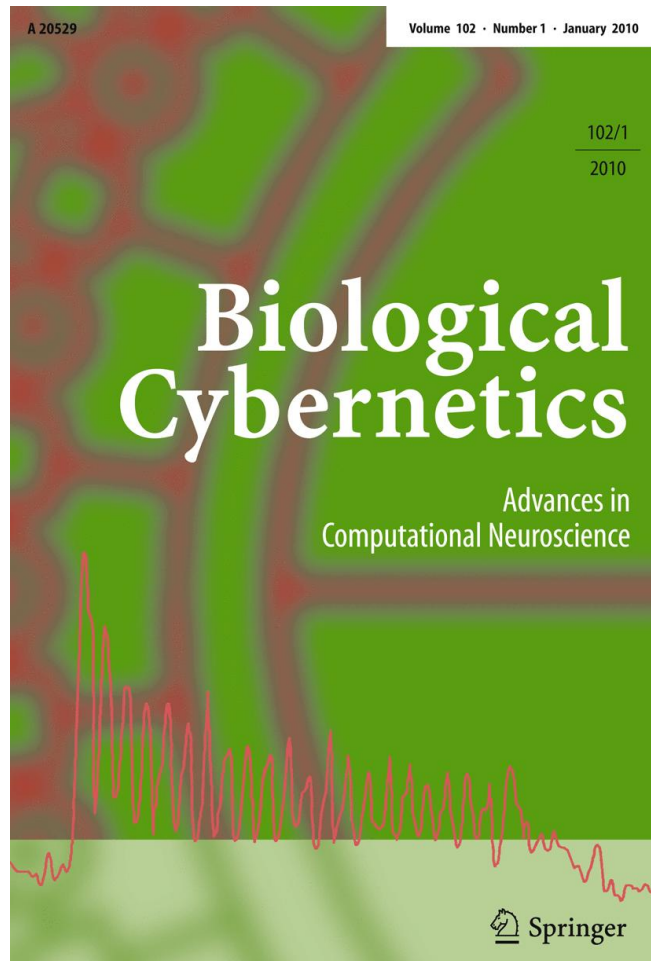


ISSN 0340-1200, Volume 102, Number 1



**This article was published in the above mentioned Springer issue.
The material, including all portions thereof, is protected by copyright;
all rights are held exclusively by Springer Science + Business Media.
The material is for personal use only;
commercial use is not permitted.
Unauthorized reproduction, transfer and/or use
may be a violation of criminal as well as civil law.**

Concurrent adaptation of force and impedance in the redundant muscle system

Keng Peng Tee · David W. Franklin · Mitsuo Kawato ·
Theodore E. Milner · Etienne Burdet

Received: 27 July 2009 / Accepted: 2 November 2009 / Published online: 21 November 2009
© Springer-Verlag 2009

Abstract This article examines the validity of a model to explain how humans learn to perform movements in environments with novel dynamics, including unstable dynamics typical of tool use. In this model, a simple rule specifies how the activation of each muscle is adapted from one movement to the next. Simulations of multijoint arm movements with a neuromuscular plant that incorporates neural delays, reflexes, and signal-dependent noise, demonstrate that the controller is able to compensate for changing internal or environment dynamics and noise properties. The computational model adapts by learning both the appropriate forces and required limb impedance to compensate precisely for

forces and instabilities in arbitrary directions with patterns similar to those observed in motor learning experiments. It learns to regulate reciprocal activation and co-activation in a redundant muscle system during repeated movements without requiring any explicit transformation from hand to muscle space. Independent error-driven change in the activation of each muscle results in a coordinated control of the redundant muscle system and in a behavior that reduces instability, systematic error, and energy.

Keywords Hybrid force-impedance control · Learning · Iterative and nonlinear adaptive control · End-effector redundancy · Muscle-space · Optimization

K. P. Tee · E. Burdet
Department of Mechanical Engineering, National University of
Singapore, Singapore, Singapore

K. P. Tee
Institute for Infocomm Research, A*STAR, Singapore, Singapore

D. W. Franklin
Department of Engineering, Cambridge University, Cambridge,
UK

D. W. Franklin
National Institute of Information and Communications
Technology, Keihanna Science City, Kyoto, Japan

D. W. Franklin · M. Kawato
Computational Neuroscience Laboratories, ATR International,
Kyoto, Japan

T. E. Milner
Department of Kinesiology and Physical Education, McGill
University, Montreal, Canada

E. Burdet (✉)
Department of Bioengineering, Imperial College, London, UK
e-mail: e.burdet@imperial.ac.uk
URL: <http://www.bg.ic.ac.uk/staff/burdet>

1 Introduction

While recent studies have shown that tool usage is not restricted to human activities (De Waal 1999; Weir et al. 2002), the exceptional capability of humans to learn to use a wide array of tools is still poorly understood. For example, how is it possible to create intricate sculptures, which require the ability to control the direction and magnitude of the force applied to a chisel as well as the ability to stabilize the chisel in the face of irregularities in the resistance of the material and noise in the commands sent to the muscles (Slifkin and Newell 1999; Osu et al. 2004)? Skills which require compensation for mechanical instability, such as sculpting, appear particularly difficult to learn as any small perturbation can lead to unpredictable and inconsistent outcomes (Burdet et al. 2006).

In order to perform these activities successfully, the central nervous system (CNS) must learn to compensate for mechanical instability as well as interaction forces arising from the environment (Burdet et al. 2001; Franklin et al. 2003a). What is the computational mechanism of this learning? Optimization algorithms such as used in (Burdet and Milner 1998;

Harris and Wolpert 1998; Stroeve 1999; Todorov and Jordan 2002; Guigon et al. 2007; Trainin et al. 2007; Izawa et al. 2008) only predict final learning outcomes, while models created to predict gradual changes of force during adaptation (Kawato et al. 1987; Katayama and Kawato 1993; Gribble and Ostry 2000; Thoroughman and Shadmehr 2000; Donchin et al. 2003; Emken et al. 2007) do not possess a mechanism to counteract mechanical instability and do not accurately predict the evolution of muscle activation observed during human motor learning (Franklin et al. 2003b).

We have recently introduced an algorithm which accounts for the ability of the CNS to improve motor skills with practice by iteratively adjusting motor commands (Franklin et al. 2008). This model is based on a simple V-shaped learning function which stipulates how feedforward commands to individual muscles are adjusted based on error, from one movement to the next. Computer simulations of movements which require compensation for instability normal to the trajectory have demonstrated that this algorithm can modify patterns of muscle activation during training to precisely counteract the effects of unstable environmental dynamics (Burdet et al. 2001; Franklin et al. 2003b).

However, the model was not rigorously tested in Franklin et al. (2008). For example, many activities require simultaneous control of force and impedance. Since this has been investigated empirically (Osui et al. 2003), data exist for comparison of model predictions with experimental observations. Similarly, model predictions can be compared to experimental observations in studies where the strength (Franklin et al. 2004) or the direction (Franklin et al. 2007a) of an instability was varied. In order to test the general validity of this model, it is necessary to examine its ability to accurately predict how patterns of muscle activation are adjusted under a broad range of conditions.

Given that there is considerable redundancy in the musculoskeletal system, does our model select and use muscles in the same way as the central nervous system? In order to address this question, we have chosen to examine a multi-joint arm movement constrained between two target positions (Scheidt et al. 2000). Since the intended movement could be produced by many combinations of the shoulder, elbow and biarticular flexor and extensor muscles this provides an appropriate test of the model.

This article first defines the model thoroughly, and investigates its generality by testing the capacity to adapt patterns of muscle activation for movements in representative force fields. We examine predictions for concurrent learning of force and impedance, the ability of the algorithm to deal with a redundant muscle system and to optimize impedance for different levels and directions of instability.

The model parameters are identified under one condition, after which computer simulations of learning are performed and compared to experimental data. We then analyze the

outcomes, as well as the predicted transients of learning in various dynamic environments, and examine the change of patterns of muscle tension, reciprocal activation and co-activation, as well as the trajectories and impedance which accompany this learning, and compare the features of the simulated results with the experimental data.

2 Heuristics of motor adaptation

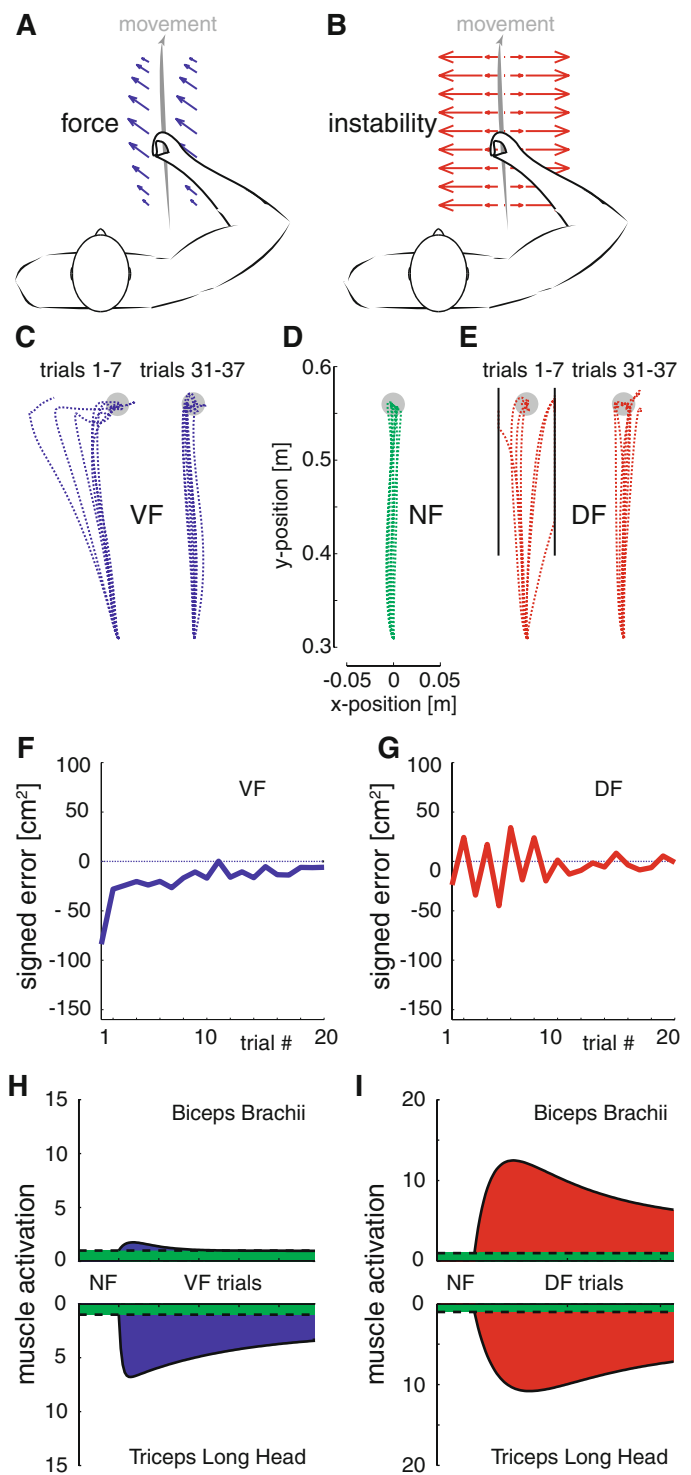
Movements repeated under similar conditions are characterized by regular patterns. We interpret these movement features as the output of mechanical plant controlled by descending *feedforward motor commands*. The muscle activation produced by learned feedforward commands is combined with activation arising from sensory feedback loops to enable us to perform skillful movements despite long sensory delays. For example, when environmental dynamics are unexpectedly altered during fast reaching movements, the trajectory is markedly disturbed immediately following the alteration, but it gradually recovers in a convergent manner with repetition. This section presents and analyzes the results of previous experiments on motor adaptation to determine how feedforward commands are modified from one movement to the next (Burdet et al. 2001; Osui et al. 2003; Franklin et al. 2003b).

Figure 1 illustrates the evolution of trajectories and muscle activation during learning of a stable interaction produced by a velocity-dependent force field (VF, Fig. 1a), and during learning of an unstable interaction produced by a position dependent divergent force field (DF, Fig. 1b). Trajectories for reaching movements ahead of the body in the VF and DF are compared to null field (NF) movements which are approximately straight (Fig. 1c, d, e). The corresponding signed errors, the directional area between the paths of each VF or DF trajectory and the mean NF trajectory for 5 subjects are shown in Fig. 1f, g.

In the velocity-dependent force field (VF) the trajectories during initial trials, which deviate to the left as a consequence of the effect of the velocity-dependent force, converge in a monotonic fashion to the NF mean trajectory (Fig. 1f). This indicates that the CNS reduces kinematic error by compensating for the perturbing effect of the environmental dynamics.

The evolution is more complex in an unstable interaction (DF). Due to motor noise, the first trial deviates left or right from the path of the mean trajectory (Fig. 1g). The instability amplifies the deviation, and the hand is pushed away from the target. Subsequent trials in the DF alternate left and right from the NF trajectory, and later movements slowly converge to it. The evolution in the initial trials suggests that, in the unstable condition also, the control is modified to reduce the kinematic error from trial to trial. After a trial in which the movement deviated to the left, the controller modifies the

Fig. 1 Adaptation to representative stable and unstable dynamics (Osu et al. 2003). **d** Shows point-to-point movements in the null field (NF). In the velocity-dependent force field (VF), the force exerted on the hand is always in the same direction (**a**). In contrast, the interaction with the unstable position dependent divergent force field (DF) is unpredictable due to motor noise (**b**). In the VF (**c**), the CNS can monotonically correct for the disturbance, while in the DF (**e**) the corrective actions lead to errors that alternate between the left and right of a straight line to the target (**d**). **f, g** show the mean integrated hand path error of five subjects in the first 20 trials, (**h, i**) a fit with two exponential functions of the evolution of (rectified and integrated) muscle activity during learning (Franklin et al. 2003b)

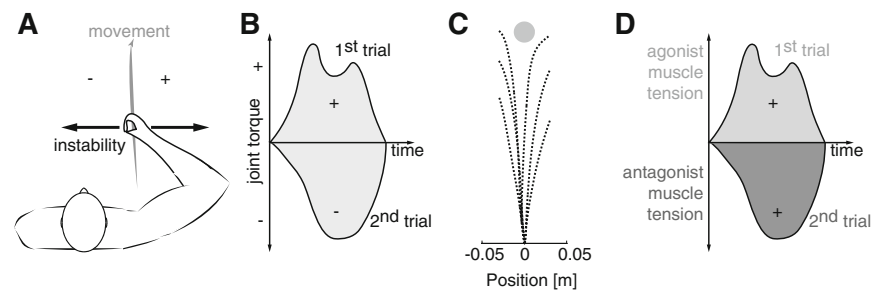


feedforward command to push to the right on next trial. This results in a movement deviating to the right. Consequently, the controller then modifies the feedforward command to push to the left, etc., resulting in the alternate movement patterns observed.

It is not obvious how the initial alternating behavior leads to stability and how the movements eventually come to resemble those made in the NF. If the CNS attempted to correct for

the error experienced in one trial by producing an opposing force on the next trial the hand path should continue to alternate to the right and left of the mean trajectory (Fig. 2a). On average, there would be no modification of torque with this strategy if the movements were distributed symmetrically on each side. Simulation of this strategy in the DF (Burdet et al. 2006), shown in Fig. 2c, confirms that it cannot lead to movements that resemble NF movements.

Fig. 2 Analysis of iterative learning principle in unstable DF dynamics performed in joint space (b) versus muscle space (d). The signed areas are defined in (a). c Shows that simulation of joint space iterative learning does not lead to successful performance even after 100 trials (Burdet et al. 2006)



Understanding how learning occurs under conditions of unstable dynamics requires analysis in muscle space. Consider two antagonistic muscles spanning a joint and producing torque in opposite directions (Fig. 2b). Muscles can only pull, i.e., muscle tension is always positive. Assuming that movement error on one trial is compensated by an opposing force on next trial, errors to the left and right from the mean trajectory will lead to a pattern of alternating increases in activation in two muscles, i.e., to co-activation (Fig. 2d). As muscle impedance increases with activation (Gomi and Osu 1998), compensation of the external force coupled with the instability will increase impedance and make the motion more stable.

Stability is also brought about by an increase in muscle activity in response to shortening in the previous movement. We can observe this particularly well in the adaptation to the VF shown in Fig. 1h, though the same process occurs in unstable interactions (Franklin et al. 2008). In the VF, activity increases in the biceps brachii, though only the antagonist triceps long head was stretched as the trajectory remained to the left of the NF path. Thus, the increase of muscle activity both after shortening and stretch stiffen the arm gradually, thereby increasing stability during movement, and improve performance.

However, muscle activity cannot increase indefinitely. In fact, examination of EMG during learning (Fig. 1h, i) shows that, both under stable and unstable conditions, muscle activity gradually decreases after an initial increase in all muscles (Franklin et al. 2003b). Direct measurement of stiffness during different phases of learning confirms that superfluous impedance is gradually eliminated (Franklin et al. 2004).

3 Model

As analyzed in previous section, the observations of learning patterns in Shadmehr and Mussa-Ivaldi (1994), Burdet et al. (2001), Franklin et al. (2003b), Milner and Franklin (2005) suggest the following *principles of motor adaptation*:

1. Motor commands in order to perform a desired action are composed of both the feedforward command, defined as the component of the motor command learned by repeating an activity, and the feedback command.

2. The feedforward command is updated from one movement to the next in muscle space as changes in the neural activation of muscles.
3. This modification of the feedforward command tends to reduce motion error experienced in the previous movement.
4. Either muscle stretch or shortening leads to augmentation of muscle activity on the following movement.
5. Muscle activation is reduced with learning.

Formulating the first principle in quantitative terms, we assume that each of the motor commands $\mathbf{w} \equiv (w_1 \cdots w_i \cdots w_N)^T$ for the N muscles involved in a movement is composed of a feedforward term \mathbf{u} , corresponding to learned dynamics, and a feedback term \mathbf{v} :

$$\mathbf{w} = \mathbf{u} + \mathbf{v}. \quad (1)$$

The neural feedback or reflex term \mathbf{v} depends on motion error \mathbf{e} . In the simulation of this article, it was modeled as

$$\mathbf{v}(t) = r(\mathbf{e}(t - \phi) + r_d \dot{\mathbf{e}}(t - \phi)) \quad (2)$$

where $r, r_d > 0$, and ϕ are the feedback delays. \mathbf{e} is the difference between the expected position and the position that results from the interaction with the environment, in coordinates of muscle length. A filtered version of this signal will be available to the CNS through afferent feedback (such as muscle spindles). In order to perform the simulations of this article, we assumed a reference trajectory λ_o , and that \mathbf{e} is the difference between the actual and this reference muscle length:

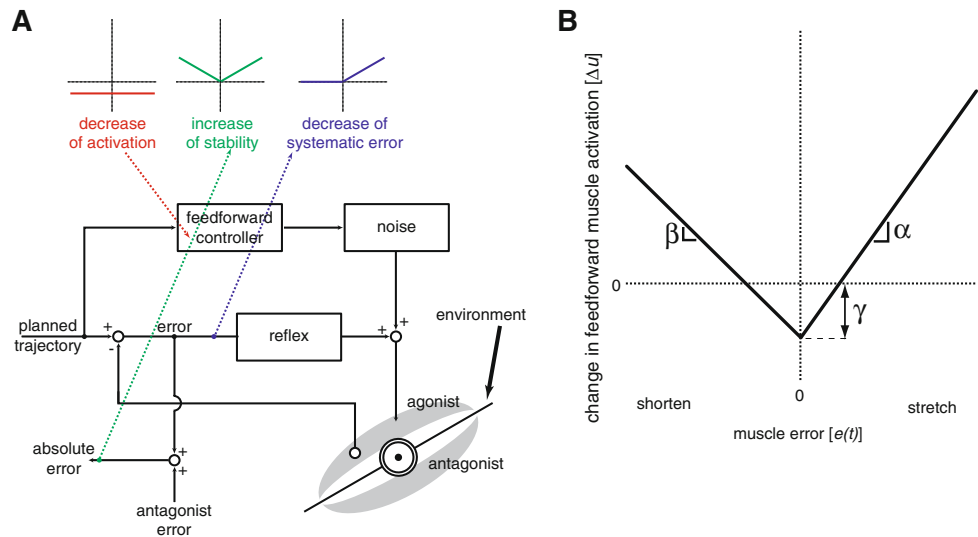
$$\mathbf{e} = \lambda - \lambda_o. \quad (3)$$

The feedforward motor command for each muscle i is then updated from one trial u_i^k to the next u_i^{k+1} by (considering that it must remain positive):

$$\begin{aligned} u_i^{k+1}(t) &\equiv \left[u_i^k(t) + \Delta u_i^k(t + \phi) \right]_+, \quad [\cdot]_+ \equiv \max\{\cdot, 0\} \\ \Delta u_i^k(t) &= \alpha \varepsilon_{i,+}^k(t) + \beta \varepsilon_{i,-}^k(t) - \gamma, \quad [\cdot]_- \equiv [-\cdot]_+ \\ \varepsilon_i^k(t) &= e_i^k(t) + g_d \dot{e}_i^k(t), \quad \alpha > \beta > 0, \quad \gamma, g_d > 0, \end{aligned} \quad (4)$$

where $e_i(t)$ is the stretch/shortening in muscle i at time t , and Δu is phase advanced by $\phi > 0$, which is equal to the

Fig. 3 The learning algorithm. **a** The control diagram illustrates local learning in each muscle corresponding to the stated principles of motor adaptation, which control force and impedance in the limbs at the point of contact with the environment. **b** The function used to adapt activation independently in each muscle



feedback delay. This *learning function*, which governs how the activity of each muscle is adapted corresponds well to the adaptation function observed in experimental data (Franklin et al. 2008). A control diagram of the overall learning is given in Fig. 3.

We note that the model of Eqs. 1 and 4 does not require a desired trajectory planned by the CNS, but only an error signal from the muscle sensors, possibly processed by the CNS. In order to examine the viability and generality of this learning controller, simulations were performed under various conditions for the same forward planar movement as in the experiments of Burdet et al. (2001), Franklin et al. (2003a,b). The two-joint six-muscle model used for simulations has redundant muscles and nonlinear dynamics. We computed adaptation of muscle tension at the output of the contractile element, i.e., the force produced by muscles on the skeleton, as described in Appendices A.1–A.3.

The physical model of the arm considered the rigid body dynamics, muscle intrinsic impedance, neural feedback, and signal-dependent motor noise as described in Appendices A.1 and A.2. The parameters for the arm: the limb lengths, masses and moments of inertia, feedback gains, feedback delays, and muscle moment arms were selected from the literature. Muscle stiffness and noise parameters were selected to produce null field (NF) movements and initial movements in the VF and the DF of Fig. 1 with trajectories and endpoint stiffness similar to those recorded experimentally. This same set of parameters was then used in all simulations.

4 Results

4.1 Concurrent regulation of force and impedance

We first simulated a rotated DF (rDF) and a rotated convergent field (rCF), previously used to study human adaptation (Osu et al. 2003), as defined by the following equation:

$$\begin{bmatrix} F_x \\ F_y \end{bmatrix} = \zeta (x \cos \theta + (y - 0.31) \sin \theta) \begin{bmatrix} \cos \theta \\ \sin \theta \end{bmatrix}, \quad (5)$$

where $\theta \equiv 7^\circ$, $(F_x, F_y)^T$ is the force (in Newtons) exerted on the hand during movement, and $(x, y)^T$ is the hand position relative to the shoulder in meters. $\zeta = 450$ N/m for rDF, and $\zeta = -450$ N/m for rCF. These force fields are designed to require the same force along the straight line movement to the target. However the rDF requires compensation for the environment instability to succeed in reaching the target while the rCF defines a stable trajectory.

We see in Fig. 4a, b that the algorithm is able to learn to compensate for both interactions. In particular, it is able to acquire the stability necessary to succeed in the unstable rDF. Furthermore, the after effects occur in the same direction under both conditions, indicating compensation of the bias force. This is further supported by the similar joint torques which were learned in each force field Fig. 4d. What is most critical for the validity of the model is that the after-effect trajectories deviate less in rDF, as was observed in the experimental results (Osu et al. 2003), indicating larger limb impedance in the rDF (Fig. 4a, b).

Figure 4c shows how the algorithm modified the distribution of integrated lateral errors after learning. The narrow distribution in the rCF has a bias which is zeroed with learning. The broader initial distribution in the rDF (compare Fig. 4a, b), spreads because the instability amplifies error, and becomes narrower and unbiased with learning.

4.2 Control of redundancy

Analysis of force adaptation was performed in Scheidt et al. (2000) by observing the modification of force against the walls of a virtual channel after a lateral VF

$$\begin{bmatrix} F_x \\ F_y \end{bmatrix} = \begin{bmatrix} -15 \dot{y} \\ 0 \end{bmatrix} \quad (6)$$

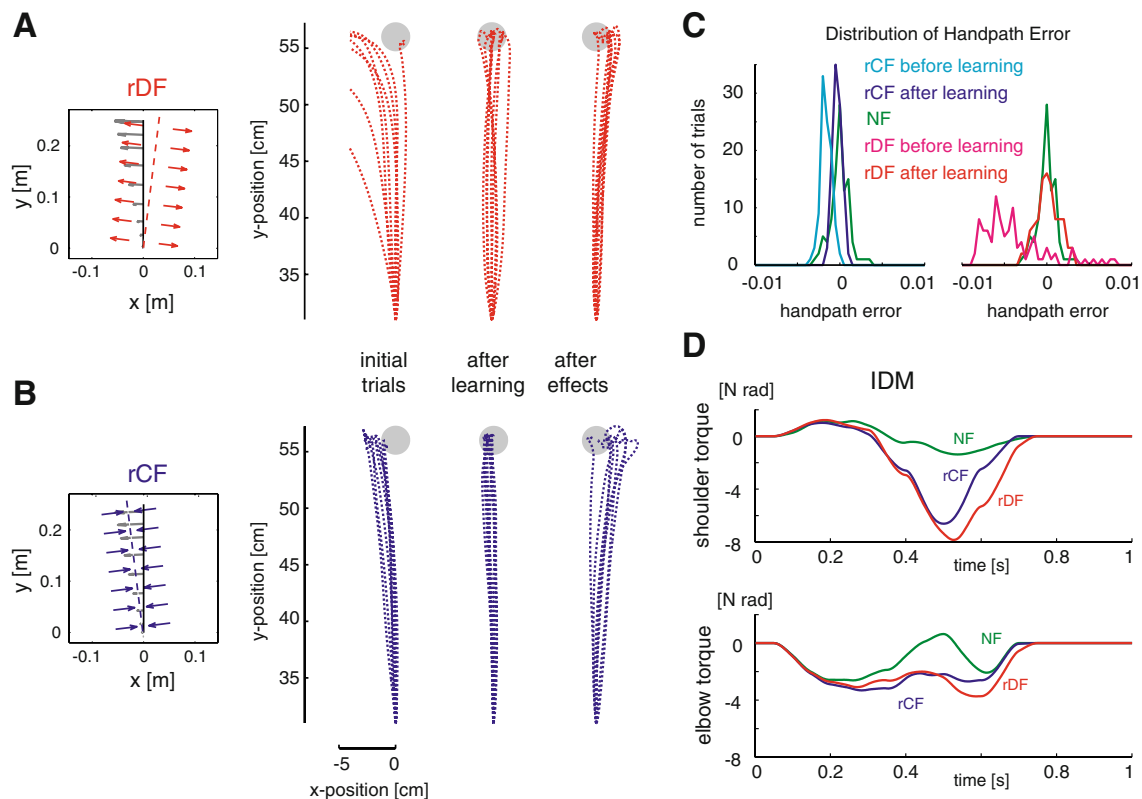


Fig. 4 Concurrent regulation of force and impedance. **a** Adaptation to the rotated divergent field (rDF). The force field (red) and forces experienced (dark gray) along the straight line to the target (black line) are shown at the left. To the right are plotted the simulated trajectories both early and late in learning, and during aftereffects. **b** Adaptation to the

rotated convergent field (rCF). **c** The distribution of (integrated lateral) hand path errors (Osui et al. 2003) for 100 movements before and after learning (when the learning factor was set to 0). **d** The joint torques in the NF, rDF, and rCF after learning

had been learned (the force is in N and velocity in m/s). The channel was implemented as a stiff lateral spring with $6000 N/m$ stiffness and $60 Ns/m$ damping to avoid oscillations.

Two particularly interesting features of this experiment are that (i) almost no kinematic error is available for (un)learning in the channel, and (ii) because of the mechanical constraint introduced by the channel the end effector's positioning system has considerable redundancy, i.e., this movement could be driven using various combinations of the shoulder, elbow, or biarticular flexor and extensor muscles.

Figure 5 shows a gradual decrease of force toward the initial NF value when the force field is replaced by the channel. In contrast, the force decreases almost immediately to the initial NF value when the force field is replaced by the NF, i.e., when kinematic error is available to the controller on every trial. This is similar to the behavior observed in Scheidt et al. (2000), and suggests that motor learning is guided by the kinematic error. The rate of decrease of force is somehow larger in the simulations than that observed in Scheidt et al. (2000), but similar to recent experimental results (Melendez-Calderon et al. 2009).

There are several interesting features in the evolution of the muscle activation predicted by the model. These include predictions that the activity of shoulder flexors and biarticular muscles increases immediately after the force field is replaced by the NF, and that this activity decreases gradually in the NF. It is also interesting to note that the biarticular extensor activity decreases rapidly when the force field is replaced by the channel, although the activity of other muscles only gradually decreases. Test performed on these predictions of the model could be used to validate the choice of learning parameters.

Another prediction is that stiffness decreases laterally while repeating movements in the channel, as working against intrinsic instability is not needed. This is produced mainly by a decrease of double joint muscle's activity.

4.3 Impedance compensates precisely for the environment instability

In order to investigate how the impedance of the arm is adapted to the impedance of the environment, we first

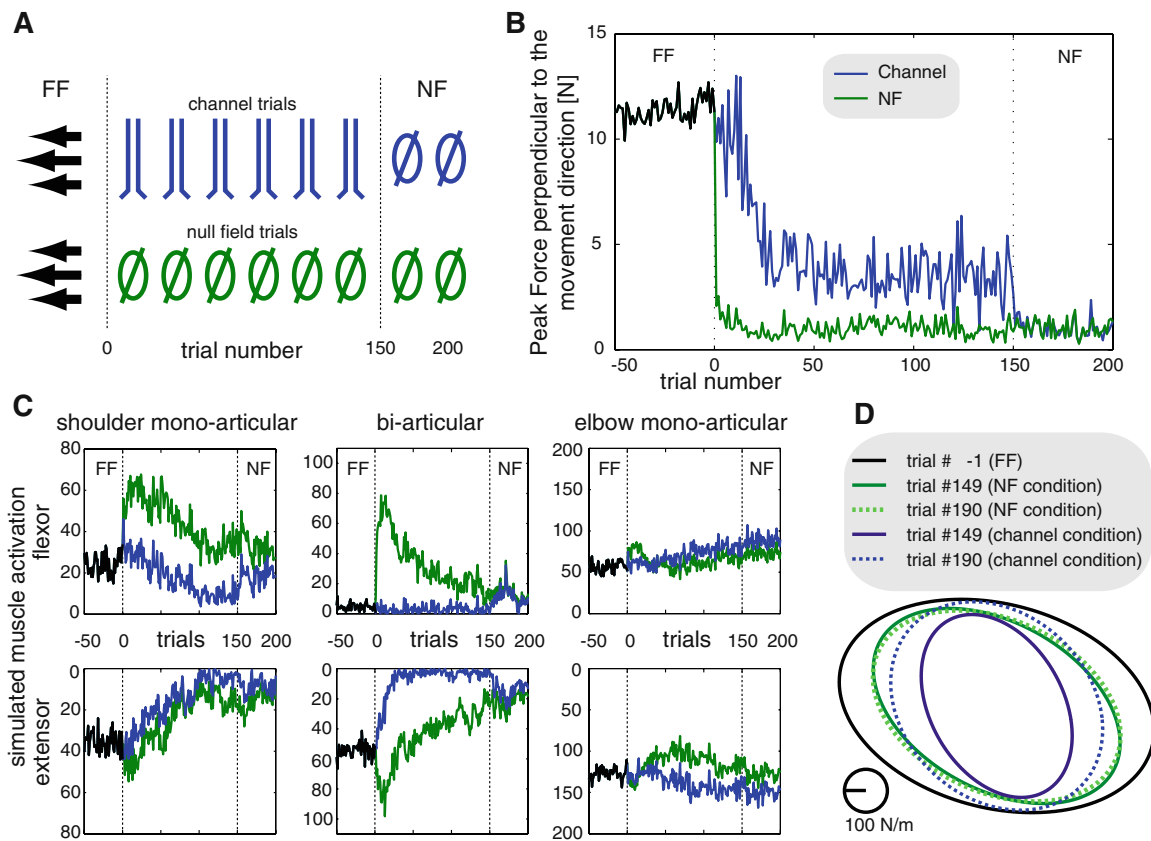


Fig. 5 Control of redundancy. **a** The simulated experimental design. Two different conditions were tested after the model had previously been adapted to the VF of Eq. 6. The field was either replaced by a channel, or an NF for 150 trials. Finally, all conditions ended with the NF. **b** Evolution of peak lateral force perpendicular to the movement direction. **c** Evolution of integrated muscle activity. Note that on the

channel trials, the muscle activity does not converge to the level found in the NF. Instead, the activity of several of the muscles decrease to below the NF levels as they are no longer required to guide the movement. **d** The endpoint stiffness ellipses for five different conditions. The stiffness is reduced in the channel not only relative to the VF but also relative to the NF

simulate the adaptation in divergent force fields (DFs) while varying the direction of instability as was done in the experiments of Franklin et al. (2007a). Specifically, we simulate learning in DFs defined by

$$\begin{bmatrix} F_x \\ F_y \end{bmatrix} = \zeta \begin{bmatrix} \cos \theta \\ \sin \theta \end{bmatrix} x, \tag{7}$$

with the force in N , orientations $\theta = -45^\circ, 0^\circ, 45^\circ$, and 80° anticlockwise, and field strengths $\zeta = 360, 450, 360$, and 225 N/m , respectively.

The learning algorithm predicts trial-by-trial changes in muscle activity (Fig. 6e) consistent with the results of Franklin et al. (2003b). The level and time course of simulated muscle activity changes in a similar fashion to muscle activity recorded during human adaptation. All the muscles increase activation after the introduction of the force field. The muscle activity peaks, and gradually reaches a plateau level, similar to that of the experimental data.

The simulated stiffness after learning (Fig. 6b) corresponds well to the mean stiffness of the subjects in Franklin et al. (2007a) (Fig. 6a). The orientation, shape, and size of the stiffness ellipses predicted by the model match the experimental data very well in most cases (Fig. 6c, d).

The analysis of muscle activation reveals that differences in stiffness are due to differentiated involvement of the muscle pairs spanning the two joints (Fig. 6e), as in the experiment (Franklin et al. 2007a). Both DF_0 and DF_{-45} require mainly co-activation of the bi-articular muscles to compensate for the instability. However, adaptation to DF_{45} and DF_{80} is produced by bi-articular and elbow muscles. DF_{80} requires particularly strong co-activation of elbow muscles, which is consistent with the geometry of these muscles, i.e., displacement along the direction of the instability is resisted primarily by length changes in these muscles.

We then simulated learning when the strength of the lateral instability was varied as in Franklin et al. (2004), by using the field of Eq. 7 with $\theta = 0$ and the field strength $\zeta = 200$,

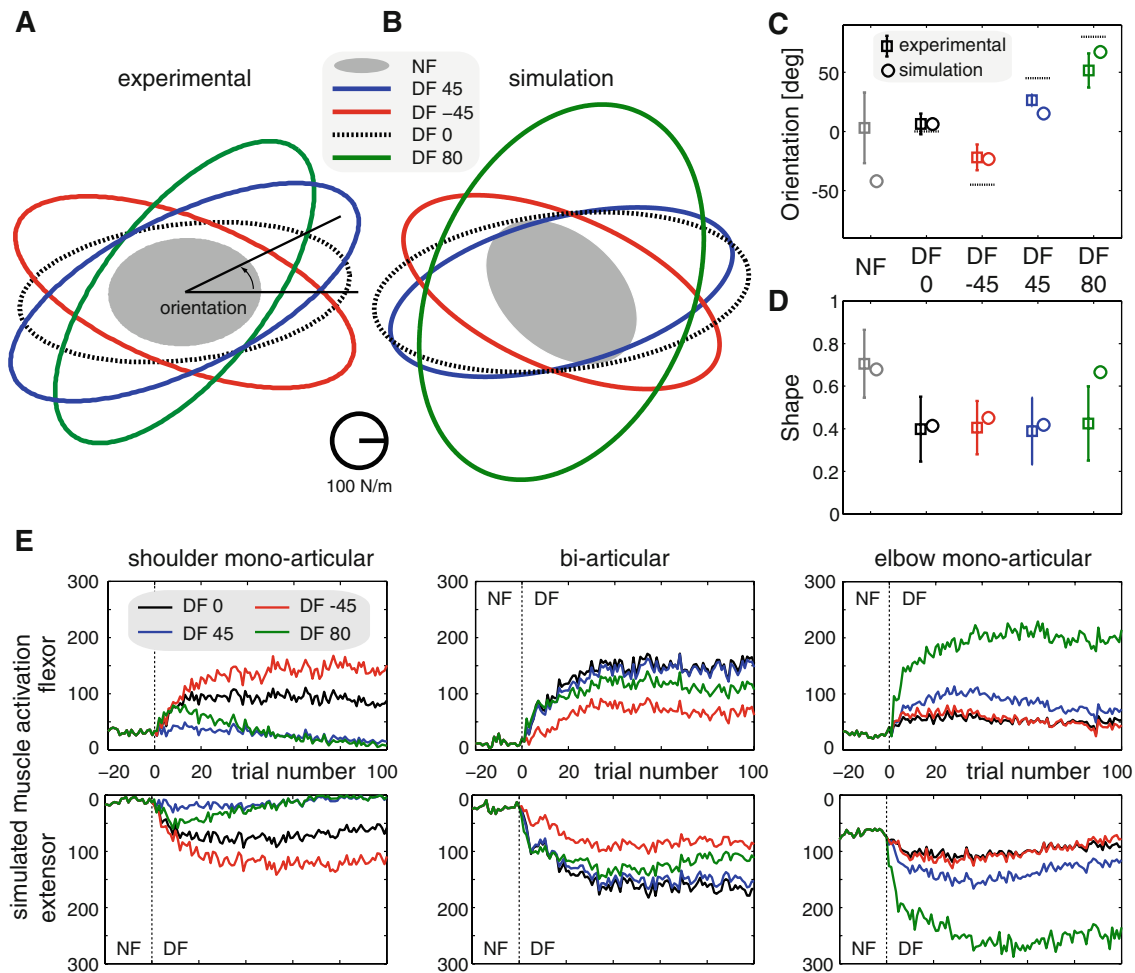


Fig. 6 Adaptation to environments with instability of different orientations. **a** Experimental endpoint stiffness of the arm after adaptation to five force fields, four of which represent environments with mechanical instability in different directions. Ellipses are derived from the mean stiffness of the subjects in Franklin et al. (2007a). **b** Simulated endpoint stiffness of the arm after learning the same five force fields. **c** A compar-

ison of the orientation of the stiffness ellipse between the experimental and simulated stiffness. **d** The shape of the endpoint stiffness ellipse, defined as the ratio of small to large axes. **e** Transients of muscle activation during learning in the environments with instability in various directions

300, 400, and 500 N/m. We see in Fig. 7 that learned stiffness increases monotonically with the strength of the environmental instability as observed experimentally (Franklin et al. 2004). Net stiffness, the difference between the overall stiffness and the environmental stiffness, reaches the same level as in NF independent of the environmental stiffness level. This means that both the simulated and biological controllers adapt to keep a similar stability margin (of about 300 N/m) under all conditions.

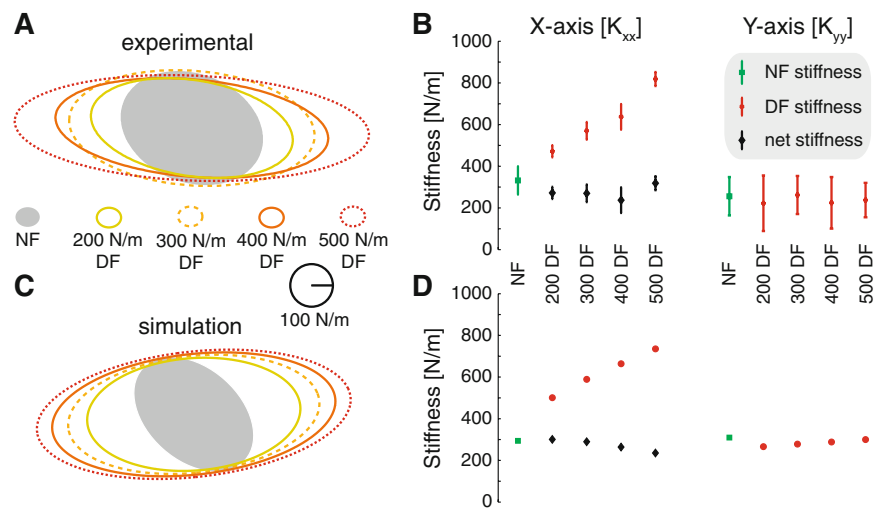
4.4 How does the CNS deal with noise?

The amount of motor noise with which the CNS must contend varies naturally among healthy individuals and increases with age (Sturman et al. 2005; Newell et al. 2006). It also increases

in pathological states such as cerebellar disorders. How does neural control adapt to such differences? Our model can be used to compare adaptation under conditions of different levels of motor noise. We investigated adaptation to an unstable force field with an instability normal to the movement direction, using a divergent force field with $\theta = 0$ and $\zeta = 450$ N/m in Eq. 7.

In our simulations, endpoint stiffness grows with the noise level both in the NF and the DF (Fig. 8a), due to a generalized increase in the activation of all muscles. Furthermore, the increase of the K_{xx} term is larger in the DF than in the NF (Fig. 8b), but similar for the other components of the stiffness matrix. Adaptation to the DF requires an increase in stability along the x -direction, which is achieved by increasing motor commands to muscles which change their length

Fig. 7 Adaptation to environments with instability of different magnitudes. **a** Mean endpoint stiffness ellipses from the data of Franklin et al. (2004). **b** Mean and standard deviations of the experimental stiffness along the x -axis (K_{xx}) and y -axis (K_{yy}) for each level of instability (Franklin et al. 2004). The net stiffness is the difference between the learned stiffness and the force field strength. **c** Simulated endpoint stiffness ellipses for each level of instability. **d** Simulated stiffness along the x - and y -axes



in response to disturbances along this direction. In turn, this increases the (signal-dependent) noise for movements in this direction, requiring a greater increase in K_{xx} in the DF than in the NF. Impedance is able to stabilize the noisy plant as it grows faster as a function of the motor command than the motor noise (Selen et al. 2005).

While this increase in endpoint limb stiffness with increasing internal motor noise has not been experimentally confirmed, a similar effect has been demonstrated under movements in the absence of visual feedback (Franklin et al. 2007b). When subjects performed movements in the unstable environment (DF), the endpoint stiffness was larger under conditions where visual feedback was absent compared to when it was present. Our conclusion is that this condition increased the uncertainty about the current state of the limb, which is required to modulate the endpoint stiffness along the trajectory under conditions of environmental instability. In order to compensate for this increased uncertainty (or increased sensory noise), the limb stiffness was increased (Franklin et al. 2007b). Such effects are comparable to the modeled changes in endpoint stiffness under the conditions of increased motor noise found here.

5 Discussion

Biological motor control is fundamentally adaptive, and it is critical to possess predictive tools with similar adaptation properties to understand the mechanisms of impairments arising from motor disorders and to facilitate rehabilitation (Emken et al. 2007). The model of motor learning presented in this article regulates the endpoint force and impedance of the arm in a manner that is similar to that observed in humans. It does this by adapting each muscle's feedforward command using a few simple principles which we deduced from observations made during psychophysical experiments.

Trial by trial adaptation was implemented with a V-shaped function of kinematic error (Franklin et al. 2008), which generates an increase in muscle activation for a stretched muscle, a smaller increase in activation for a shortened muscle, and a decrease in activation for small kinematic errors. This model is fundamentally different from previous models based on iterative and adaptive control (Kawato et al. 1987; Katayama and Kawato 1993; Gribble and Ostry 2000; Thoroughman and Shadmehr 2000; Donchin et al. 2003; Emken et al. 2007; Schweighofer et al. 1998; Thoroughman and Taylor 2005) and corresponding nonlinear adaptive controllers for robots (Slotine and Li 1991; Bien and Xu 1998; Burdet et al. 1998) as it is equipped with a mechanism to adapt impedance and can successfully stabilize unstable dynamics.

The asymmetrical V-shaped adaptation law, Eq. 4, can be decomposed into an antisymmetric proportional function, a symmetric function and a negative bias:

$$\begin{aligned} \Delta u^k &= \alpha \varepsilon_+^k + \beta \varepsilon_-^k - \gamma, \quad \alpha > \beta > 0, \quad \gamma > 0, \\ &= \frac{1}{2}(\alpha + \beta)|\varepsilon^k| + \frac{1}{2}(\alpha - \beta)\varepsilon^k - \gamma, \end{aligned} \quad (8)$$

where the muscle index and time have been dropped for simplicity. In this representation, the first term $|\varepsilon|$ increases co-activation in response to deviation, i.e., increases stability; the second term ε produces a force opposed to the error, i.e., compensates for systematic error; and the third term $-\gamma$ removes superfluous activation. Therefore, *the adaptation of Eq. 4 concurrently increases stability, decreases movement error, and decreases effort.*

The modeled controller used those parameters which were fixed after matching behavior observed under the NF condition and during adaptation to the VF used in Franklin et al. (2003a). It is remarkable that this single set of parameters leads to successful performance of multijoint reaching arm movements with features similar to those observed in all the experiments that we have attempted to simulate (Burdet et al.

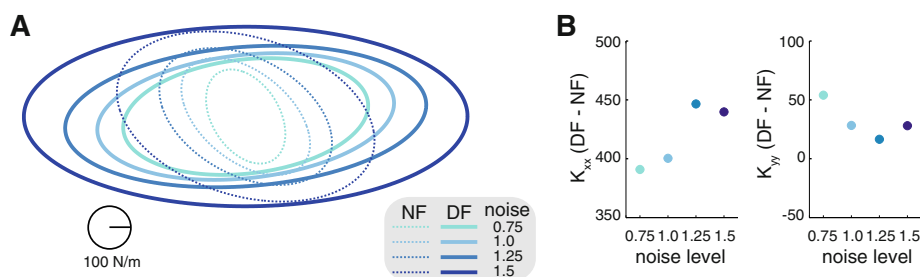


Fig. 8 Effect of different levels of signal-dependent noise. **a** Simulated stiffness ellipses in the NF and DF for four different motor noise levels. A multiplicative noise factor was used in Eq. 19 as described in

the figure. **b** The difference in the stiffness along the x -axis, (K_{xx}), and y -axis, (K_{yy}), between the DF and NF force fields for each noise level

2001; Franklin et al. 2003a,b, 2004, 2007a; Osu et al. 2003; Scheidt et al. 2000; Melendez-Calderon et al. 2009).

In particular, it was shown to accurately predict the coordination of muscles required to interact with the novel dynamics characterized by instability in various directions and of various strength, as illustrated in Figs. 6 and 7, and to predict how the CNS may adapt to increasing motor noise. We have seen that the decay rate of force matched the experimental results of Melendez-Calderon et al. (2009) but was somehow faster than that found in Scheidt et al. (2000). This may illustrate the capability of the CNS to modulate the speed of learning, i.e., the slopes and intercept of our simple algorithm, depending on the errors experienced in previous trials. Another possible explanation is the finding that there are at least two interacting adaptive processes with different time scales which are responsible for motor learning (Smith et al. 2006). Therefore, our model may mainly capture the properties of the fast adaptive process while the extremely slow decay of force seen in the experimental condition may result from the slow adaptive process.

An important aspect of our control algorithm is its ability to regulate reciprocal activation and co-activation in the redundant muscle system without requiring any explicit transformation from hand to muscle space. Movement error detected by the sensors during repeated movements provides sufficient information to coordinate the highly redundant musculoskeletal system and learn to perform movements successfully while reducing expenditure of metabolic energy, i.e., muscle activation, as demonstrated by the results shown in Fig. 5.

In contrast to previous models based on numerical optimization (Burdet and Milner 1998; Harris and Wolpert 1998; Stroeve 1999; Guigon et al. 2007; Trainin et al. 2007) or (linear) optimal control (Todorov and Jordan 2002; Izawa et al. 2008), which can be used to predict the behavior after learning, our model is able to predict how sensory information is used to modify the motor commands during the entire learning process, from one movement to the next. It may also be used to investigate convergence to a local optimum,

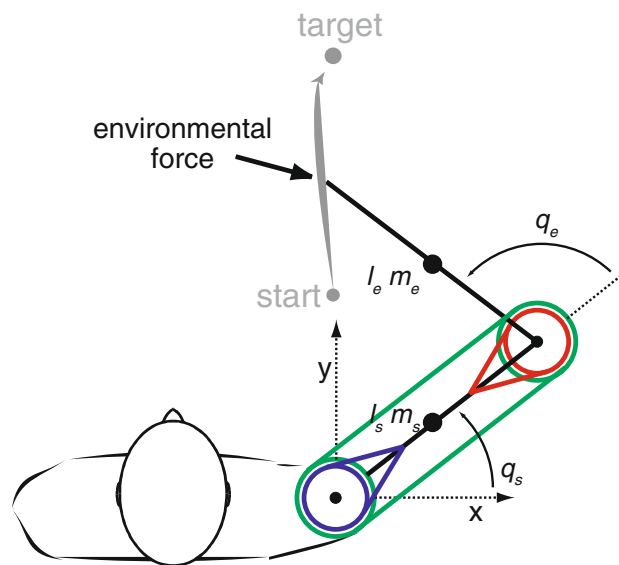


Fig. 9 Simulations of horizontal arm movements were performed using the two-joint six-muscle model described in this diagram

which occurs in tasks with multiple optima such as slalom movements (Todorov and Jordan 1998), or cases when motor learning does not converge.

Acknowledgments We thank Hamid Kaddiallah and Ganesh Gowrishankar for discussions. This work has been jointly funded by the European Commission's Seventh Framework Programme as part of the VIATORS project grant No 231554, Japan's Strategic Research Program for Brain Sciences (SRPBS), and the Natural Sciences and Engineering Research Council of Canada (NSERC).

6 Appendix

6.1 Mechanical arm model

The convention we use for the formulae of this section is that scalars s are *italic*, while vectors \mathbf{v} and matrices \mathbf{M} are bold. Figure 9 presents a schematic of the two-joint six-muscle model of the arm used in the simulation. The dynamics of

the arm moving in a horizontal plane while interacting with the environment is described (in joint space) by:

$$\tau_{RB}(\mathbf{q}, \dot{\mathbf{q}}, \ddot{\mathbf{q}}) + \mathbf{J}^T(\mathbf{q}) \mathbf{F}_E = \mathbf{J}_m^T \mathbf{m} \tag{9}$$

Muscle tensions \mathbf{m} are needed to move the limb, i.e., to produce the rigid-body dynamics τ_{RB} and counteract the external force \mathbf{F}_E , where $\tau_{RB} = (\tau_s, \tau_e)^T$ are the vectors of torque at the shoulder and elbow joints, respectively, and $\mathbf{F}_E = (F_x, F_y)^T$ represents the Cartesian vector of the force exerted on the hand. This force is transformed into joint torques using the Jacobian

$$\mathbf{J}(\mathbf{q}) = \begin{bmatrix} -l_s s_s - l_e s_{se} & -l_e s_{se} \\ l_s c_s + l_e c_{se} & l_e c_{se} \end{bmatrix}, \tag{10}$$

where $s_s \equiv \sin q_s$, $s_{se} \equiv \sin(q_s + q_e)$, $c_s \equiv \cos(q_s)$, $c_{se} \equiv \cos(q_s + q_e)$.

$\tau_{RB}(\mathbf{q}, \dot{\mathbf{q}}, \ddot{\mathbf{q}})$ are the dynamics due to inertia and velocity-dependent forces, where $\mathbf{q} = (q_s, q_e)^T$ are the vectors of shoulder and elbow joint angles, $\dot{\mathbf{q}}$ and $\ddot{\mathbf{q}}$ its first and second time derivatives, respectively. The dynamics of a two link arm model moving in the horizontal plane (Fig. 9) are:

$$\begin{aligned} \tau_{RB} &= \Omega(\mathbf{q}, \dot{\mathbf{q}}, \ddot{\mathbf{q}}) \mathbf{p} \\ \Omega_{11} &= \Omega_{21} = \ddot{q}_s + \ddot{q}_e, \quad \Omega_{12} = c_e \ddot{q}_e - s_e \dot{q}_e (2\dot{q}_s + \dot{q}_e), \\ \Omega_{22} &= c_e (\ddot{q}_s + \ddot{q}_e) + s_e \dot{q}_s^2, \quad \Omega_{13} = 0, \quad \Omega_{23} = \ddot{q}_e, \\ p_1 &= I_e + m_e l_{m,e}^2, \quad p_2 = m_e l_s l_{m,e}, \\ p_3 &= I_s + m_s l_{m,s}^2 + m_e l_s^2, \end{aligned} \tag{11}$$

where m_s and m_e are the masses of the upper arm and lower arm respectively, l_s and l_e the corresponding segment lengths, $l_{m,s}$ and $l_{m,e}$ the distances to the respective centers of mass of the segments, and I_s and I_e the respective moments of inertia.

In the experiments with human subjects, a computer-controlled force was exerted on the hand during movement by a haptic interface. The external force used in the simulations is that produced by the robotic interface, and corresponds to one of the force fields described in the main text of this article plus the dynamics of this interface as modeled in Tee et al. (2004).

The vector of muscle tensions is

$$\mathbf{m} = (m_{s+}, m_{s-}, m_{e+}, m_{e-}, m_{b+}, m_{b-})^T, \tag{12}$$

which consists of the muscle tension in the shoulder flexor (m_{s+}) and extensor (m_{s-}), elbow flexor (m_{e+}) and extensor (m_{e-}), and biarticular flexor (m_{b+}) and extensor muscles (m_{b-}). These muscle tension terms are transformed into joint torques using the Jacobian $\mathbf{J}_m(\boldsymbol{\rho})$, which is a matrix of constants comprising the muscle moment arms $\boldsymbol{\rho} = (\rho_{s+}, \rho_{s-}, \rho_{e+}, \rho_{e-}, \rho_{bs+}, \rho_{bs-}, \rho_{be+}, \rho_{be-})^T$:

$$\begin{bmatrix} \tau_s \\ \tau_e \end{bmatrix} = \begin{bmatrix} \rho_{s+} & 0 \\ -\rho_{s-} & 0 \\ 0 & \rho_{e+} \\ 0 & -\rho_{e-} \\ \rho_{bs+} & \rho_{be-} \\ -\rho_{bs+} & -\rho_{be-} \end{bmatrix}^T \begin{bmatrix} m_{s+} \\ m_{s-} \\ m_{e+} \\ m_{e-} \\ m_{b+} \\ m_{b-} \end{bmatrix}. \tag{13}$$

ρ_{s+} and ρ_{s-} are the moment arms of the shoulder flexor and extensor muscles, respectively; ρ_{e+} and ρ_{e-} the moment arms of elbow flexor and extensor muscles; ρ_{bs+} and ρ_{bs-} the moment arms of biarticular flexor and extensor muscles around the shoulder; and ρ_{be+} and ρ_{be-} their moment arms around the elbow.

6.2 Components of muscle tension

For each muscle, we assume that the tension depends on the motor command u , muscle length λ , and rate of change of length $\dot{\lambda}$:

$$m = m(\lambda, \dot{\lambda}, u). \tag{14}$$

Muscle tension is composed of two terms:

$$m = [m_A + m_{IMP}]_+, \quad [\cdot]_+ \equiv \max\{\cdot, 0\}, \tag{15}$$

where $m_A(u)$ is due to the motor command u , and m_{IMP} corresponds to mechanical impedance (the resistance to perturbation of the state) produced by muscle, i.e., to muscle stiffness and damping.

Muscle impedance is modeled as

$$m_{IMP}(t) = \kappa (e(t) + \kappa_d \dot{e}(t)), \tag{16}$$

where e is the muscle stretch/shortening, κ is the muscle stiffness, and κ_d is the ratio of muscle viscosity to stiffness. The intrinsic stiffness κ is assumed to increase linearly with the total motor command v (Hunter and Kearney 1982; Kirsch et al. 1994):

$$\kappa(t) = \kappa_0 + \kappa_1 v(t) \tag{17}$$

w represents the sum of the feedforward descending motor command from the CNS, u , inherent motor noise, u_N , and neural feedback, v :

$$w = [u + u_N + v]_+ \tag{18}$$

The overall effect of the many different sources of variance in the command is modeled as *noise* in the motor command:

$$u_N(t) = (\mu_0 + \mu_1 u) \mu(t), \tag{19}$$

where $\mu(t)$ is 0 mean Brownian motion corresponding to the deviation observed in Burdet et al. (2001). As described in Eq. 2, the neural feedback or reflex term is modeled as

$$v(t) = r (e(t - \phi) + r_d \dot{e}(t - \phi)) \tag{20}$$

where ϕ is the feedback delay. This term represents feedback from all the sources to the motoneuron, which can be excitatory or inhibitory, i.e., it can be positive or negative, respectively.

We assume that muscle tension is equal to the motor command:

$$m_A = w = [u + u_N + v]_+ \quad (21)$$

This simple muscle model has a small number of parameters, whose values can be identified from the literature. We have deliberately chosen to model force rather than activation to avoid having to model activation dynamics. Since a number of studies have measured reflex torque, estimates can be made of the feedback impedance parameters.

Note that while the model is linear in terms of the length–tension relationship, it is nonlinear with respect to its input–output relationships between command and tension. In particular, in our model muscle, impedance increases with activation (a feature critical for impedance control). Because the muscle activation level depends both on the feedforward and feedback motor commands, the tension does not depend linearly on the command.

Update of feedforward u from trial k to $k + 1$ was implemented using *learning law* Eq. 4, which we repeat here for completeness:

$$u^{k+1}(t) \equiv \left[u^k(t) + \Delta u^k(t + \phi) \right]_+, \quad (22)$$

$$\Delta u^k(t) = \alpha \varepsilon_+^k(t) + \beta \varepsilon_-^k(t) - \gamma,$$

$$\varepsilon^k(t) = e^k(t) + g_d \dot{e}^k(t), \quad \alpha > \beta > 0, \quad \gamma, g_d > 0,$$

where Δu is phase advanced by $\phi > 0$, which is equal to the feedback delay.

6.3 Simulation with physiological parameters

In our implementation, the change in muscle length was evaluated relative to a reference trajectory (Eq. 3):

$$e = \lambda - \lambda_o. \quad (23)$$

This reference trajectory, λ_o , was computed as the mean NF trajectory in 20 consecutive movements (Burdet et al. 2006; Tee 2003). It was calculated in joint space and then transformed into muscle space via inverse kinematics.

The *kinematic parameters* are based on realistic anthropometric data as shown in Table 1. The moment arms are estimates that fall within the range reported in the literature (Kuechle et al. 1997; Murray et al. 1995; Nijhof and Kouwenhoven 2000), selected to produce feedback modification mainly in the double joint muscles during initial trials in the DF such as those observed in Franklin et al. (2003b):

Table 1 Anthropometric data for arm segments

	Upper arm	Forearm
Mass (kg)	1.93	1.52
Length (m)	0.31	0.34
Center of mass from proximal joint (m)	0.165	0.19
Mass moment of inertial (kg)	0.0141	0.0188

shoulder monoarticulars : $\rho_{s+} = \rho_{s-} = 3.0$ cm

elbow monoarticulars : $\rho_{e+} = \rho_{e-} = 2.1$ cm

shoulder biarticulars : $\rho_{bs+} = \rho_{bs-} = 4.4$ cm

elbow biarticulars : $\rho_{be+} = \rho_{be-} = 3.38$ cm

The *noise* is an additive component of the muscle tension with parameters set to emulate the movement variability observed in the experimental data of NF movements and initial movements in the VF and DF. It is described by

$$\mu_0 = 7, \quad \mu_1 = 0.04, \quad \mu = 12.5 f(v) \quad (24)$$

where $v \in N(0, 1)$ is a normally distributed random variable, and $f(\cdot)$ is a causal fifth-order Butterworth filter with 2Hz cut-off frequency.

The *muscle impedance and feedback impedance parameters* were selected so that the ratio of feedback to intrinsic contribution was between 20 and 45%, corresponding to Carter et al. (1990). The delay parameter was assumed to be $\phi = 60$ ms. The ratios of damping to stiffness for the muscle and feedback components were chosen to be $\kappa_d = 1/12$ s and $r_d = 2$ s such that intrinsic muscle properties were mainly position dependent while feedback was mainly velocity dependent (Rack 1981). $\kappa_o = 3,360$ Nm⁻¹ and $\kappa_1 = 118$ m⁻¹ were chosen to obtain stiffness ellipses and initial trajectories in the VF that were representative of experimental results. $r = 336$ Nm⁻¹ produces deviation on unanticipated VF trials (before effects) of similar magnitude as in the experiments.

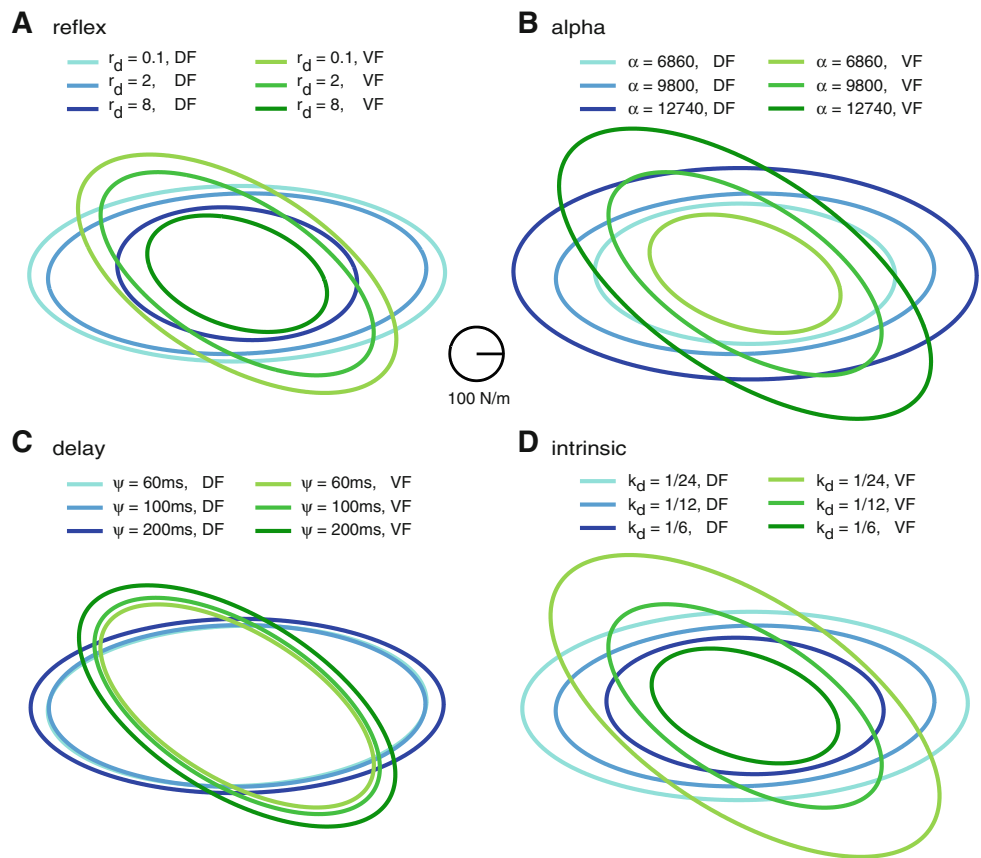
The results of Gomi and Osu (1998) show that control of tension in elbow muscles $m_{A,el}$ and in biarticular muscles $m_{A,bi}$ is linked, which we implement as

$$m_{A,el\pm} = [u_{el\pm} + u_{N,el\pm} + v_{el\pm}]_+ + 0.3 m_{A,bi\pm} \quad (25)$$

where u is described in Eq. 4 and u_N, v and m_A in Eqs. 19–21. Concerning the *learning parameters*, the ratio of the velocity- to position-dependent terms used for learning, $g_d = 0.2$, is set to correspond to the restoring force due to the combined effect of intrinsic muscle properties and neural feedback. The other parameters were chosen to achieve a steady state similar to experimental observations in the NF. At steady state, $\Delta u = 0$ thus

$$\alpha \varepsilon_{ss,+} + \beta \varepsilon_{ss,-} = \gamma \quad (26)$$

Fig. 10 Sensitivity analysis. **a** Stiffness ellipses after learning in the sDF and VF while varying the ratio of velocity to position gain of the reflex. **b** Stiffness ellipses while varying the learning factor. **c** Stiffness ellipses while varying the reflex delay. **d** Stiffness ellipses while varying the ratio of velocity to position gain of the intrinsic muscle stiffness. The shape of the stiffness ellipses was not modified by the variations of parameters



where ϵ_{ss} denotes the steady-state muscle length error. For simplicity, we assume that ϵ_{ss} is equal to the mean of the two possible values $\{\frac{\gamma}{\alpha}, \frac{\gamma}{\beta}\}$ (see Fig. 3b), i.e., $\epsilon_{ss} = \frac{1}{2}(\frac{\gamma}{\alpha} + \frac{\gamma}{\beta})$, which leads to the following equation:

$$\gamma = \frac{2 \epsilon_{ss} \alpha \beta}{\alpha + \beta} \tag{27}$$

where $\beta = 0.7\alpha$ corresponds to the data of Franklin et al. (2003b); $\epsilon_{ss} = 7.8 \times 10^{-4}$ m is based on data from NF trials; and $\alpha = 9800$ with the corresponding γ from Eq. 27 gives the correct transient behavior in the VF of Franklin et al. (2003b). This set of parameters was used in all the simulations of this article.

6.4 Sensitivity analysis

Learning was relatively insensitive to parameters different from the default values described above, as long as the movements were stable under the NF condition (Tee 2003). The resulting impedance had similar characteristics, as shown in Fig. 10, for a wide range of values of the reflex delay, ratio of velocity- to position-dependent force (from both intrinsic muscle properties and reflexes), and learning factors. The impedance remains virtually unaltered by large variations of the reflex delay. Increasing the velocity component of the reflex or intrinsic muscle force produces a decrease in the

magnitude of the impedance. Increasing the learning factor increases the magnitude of impedance.

6.5 Ethics statement

The experiments reported in this study were conducted according to the principles expressed in the Declaration of Helsinki. The study was approved by the Institutional Review Board of ATR International. All the subjects provided written informed consent for the collection of samples and subsequent analysis.

References

Bien Z, Xu JX (1998) Iterative learning control: analysis, design, integration and applications. Kluwer Academic Publishers, Boston

Burdet E, Milner TE (1998) Quantization of human motions and learning of accurate movements. Biol Cybern 78:307–318

Burdet E, Codourey A, Rey L (1998) Experimental evaluation of nonlinear adaptive controllers. IEEE Control Syst Mag 18:39–47

Burdet E, Osu R, Franklin DW, Milner TE, Kawato M (2001) The central nervous system stabilizes unstable dynamics by learning optimal impedance. Nature 414:446–449

Burdet E, Tee KP, Mareels I, Milner TE, Chew CM, Franklin DW, Osu R, Kawato M (2006) Stability and motor adaptation in human arm movements. Biol Cybern 94:20–32

Carter RR, Crago PE, Keith MW (1990) Stiffness regulation by reflex action in the normal human hand. J Neurophysiol 64:105–118

- De Waal FBM (1999) Cultural primatology comes of age. *Nature* 399:635–636
- Donchin O, Francis JT, Shadmehr R (2003) Quantifying generalization from trial-by-trial behavior of adaptive systems that learn with basis functions: theory and experiments in human motor control. *J Neurosci* 23:9032–9045
- Emken JL, Benitez R, Sideris A, Bobrow JE, Reinkensmeyer DJ (2007) Motor adaptation as a greedy optimization of error and effort. *J Neurophysiol* 97:3997–4006
- Franklin DW, Burdet E, Osu R, Kawato M, Milner TE (2003a) Functional significance of stiffness in adaptation of multijoint arm movements to stable and unstable dynamics. *Exp Brain Res* 151:145–157
- Franklin DW, Osu R, Burdet E, Kawato M, Milner TE (2003b) Adaptation to stable and unstable dynamics achieved by combined impedance control and inverse dynamics model. *J Neurophysiol* 90:3270–3282
- Franklin DW, So U, Kawato M, Milner TE (2004) Impedance control balances stability with metabolically costly muscle activation. *J Neurophysiol* 92:3097–3105
- Franklin DW, Liaw G, Milner TE, Osu R, Burdet E, Kawato M (2007a) Endpoint stiffness of the arm is directionally tuned to instability in the environment. *J Neurosci* 27:7705–7716
- Franklin DW, So U, Burdet E, Kawato M (2007b) Visual feedback is not necessary for the learning of novel dynamics. *PLoS ONE* 2(12):e1336. doi:10.1371/journal.pone.0001336
- Franklin DW, Burdet E, Tee KP, Osu R, Milner TE, Chee CM, Kawato M (2008) CNS learns stable, accurate, and efficient movements using a simple algorithm. *J Neurosci* 28(44):11165–11173
- Gomi H, Osu R (1998) Task-dependent viscoelasticity of human multijoint arm and its spatial characteristics for interaction with environments. *J Neurosci* 18(21):8965–8978
- Gribble PL, Ostry DJ (2000) Compensation for loads during arm movements using equilibrium point control. *Exp Brain Res* 135:474–482
- Guigon E, Baraduc P, Desmurget M (2007) Computational motor control: redundancy and invariance. *J Neurophysiol* 97:331–347
- Harris CM, Wolpert DM (1998) Signal-dependent noise determines motor planning. *Nature* 394:780–784
- Hunter IW, Kearney RE (1982) Dynamics of human ankle stiffness: variation with mean ankle torque. *J Biomech* 15:747–752
- Izawa J, Rane T, Donchin O, Shadmehr R (2008) Motor adaptation as a process of reoptimization. *J Neurosci* 28:2883–2891
- Katayama M, Kawato M (1993) Virtual trajectory and stiffness ellipse during multijoint arm movement predicted by neural inverse models. *Biol Cybern* 69:353–362
- Kawato M, Furukawa K, Suzuki R (1987) A hierarchical neural-network model for control and learning of voluntary movement. *Biol Cybern* 57:169–185
- Kirsch RF, Boskov D, Rymer WZ (1994) Muscle stiffness during transient and continuous movements of cat muscle: perturbation characteristics and physiological relevance. *IEEE Trans Biomed Eng* 41:758–770
- Kuechle DK, Newman SR, Itoi E, Morrey BF, An KN (1997) Shoulder muscle moment arms during horizontal flexion and elevation. *J Shoulder Elb Surg* 6(5):429–439
- Melendez-Calderon A, Masia L, Casadio M, Burdet E (2009) Force field compensation can be learned without proprioceptive error. In: Proceedings of the medical physics and biomedical engineering world congress
- Milner TE, Franklin DW (2005) Impedance control and internal model use during the initial stage of adaptation to novel dynamics in humans. *J Physiol* 567(2):651–664
- Murray WM, Delp SL, Buchanan TS (1995) Variation of muscle moment arms with elbow and forearm position. *J Biomech* 28(5):513–525
- Newell KM, Vaillancourt DE, Sosnoff JJ (2006) Aging, complexity, and motor performance. In: Birren JE, Schaie KW, Abeles RP, Gatz M, Salthouse TA (eds) Handbook of the psychology of aging. Academic Press, San Diego
- Nijhof EJ, Kouwenhoven E (2000) Simulation of multi-joint arm movements. In: Winters JM, Crago PE (eds) Biomechanics and neural control of posture and movement. Springer-Verlag, Berlin, pp 363–372
- Osu R, Burdet E, Franklin DW, Milner TE, Kawato M (2003) Different mechanisms involved in adaptation to stable and unstable dynamics. *J Neurophysiol* 90:3255–3269
- Osu R, Kamimura N, Iwasaki H, Nakano E, Harris CM, Wada Y, Kawato M (2004) Optimal impedance control for task achievement in the presence of signal-dependent noise. *J Neurophysiol* 92(2):1199–1215
- Rack PMH (1981) Limitations of somatosensory feedback in control of posture and movement. In: Brooks VB (ed) Motor control. Handbook of physiology, Sect. 1. The nervous system. American Physiological Society, pp 229–256
- Selen LPJ, Beek PJ, van Dieen JH (2005) Can co-activation reduce kinematic variability? A simulation study. *Biol Cybern* 93:373–381
- Scheidt RA, Reinkensmeyer DJ, Conditt MA, Rymer WZ, Mussa-Ivaldi FA (2000) Persistence of motor adaptation during constrained, multi-joint, arm movements. *J Neurophysiol* 84:853–862
- Schweighofer N, Spelstra J, Arbib MA, Kawato M (1998) Role of the cerebellum in reaching movements in humans. II. A neural model of the intermediate cerebellum. *Eur J Neurosci* 10:95–105
- Shadmehr R, Mussa-Ivaldi FA (1994) Adaptive representation of dynamics during learning of a motor task. *J Neurosci* 14:3208–3224
- Slifkin AB, Newell KM (1999) Noise, information transmission, and force variability. *J Exp Psychol Hum Percept Perform* 25(3):837–851
- Slotine JJ, Li W (1991) Applied nonlinear control. Prentice Hall, Englewood Cliffs, NJ
- Smith MA, Ghazizadeh A, Shadmehr R (2006) Interacting adaptive processes with different timescales underlie short-term motor learning. *PLoS Biol* 4(6):e179. doi:10.1371/journal.pbio.0040179
- Stroev S (1999) Impedance characteristics of a neuromusculoskeletal model of the human arm II. Movement control. *Biol Cybern* 81:495–504
- Sturman MM, Vaillancourt DE, Corcos DM (2005) Effects of aging on the regularity of physiological tremor. *J Neurophysiol* 93:3064–3074
- Tee KP (2003) A unified model of human motor adaptation to stable and unstable dynamics. MSc thesis, National University of Singapore
- Tee KP, Burdet E, Chew CM, Milner TE (2004) A model of endpoint force and impedance in human arm movements. *Biol Cybern* 90:368–375
- Thoroughman KA, Shadmehr R (2000) Learning of action through adaptive combination of motor primitives. *Nature* 407:742–747
- Thoroughman KA, Taylor JA (2005) Rapid reshaping of human motor generalization. *J Neurosci* 25(39):8948–8953
- Todorov E, Jordan M (1998) Smoothness maximization along a predefined path accurately predicts the speed profiles of complex arm movements. *J Neurophysiol* 80(2):696–714
- Todorov E, Jordan MI (2002) Optimal feedback control as a theory of motor coordination. *Nat Neurosci* 5:1226–1235
- Trainin E, Meir R, Karniel A (2007) Explaining patterns of neural activity in the primary motor cortex using spinal cord and limb biomechanics models. *J Neurophysiol* 97:3736–3750
- Weir AAS, Chappell J, Kacelnik A (2002) Shaping of hooks in New Caledonian crows. *Science* 297:981